JOURNAL OF MATERIALS SCIENCE 18 (1983) 447–456

Fracture behaviour of a single-fibre graphite/epoxy model composite containing a broken fibre or cracked matrix

JAYANT M. MAHISHI, DONALD F. ADAMS
Composite Materials Research Group, University of Wyoming, Laramie, Wyoming 82071, USA

A micromechanical analysis of crack initiation and propagation from a broken fibre end, or in the region of a matrix crack, in a graphite/epoxy composite model is considered. The model consists of a single fibre embedded in an annular sheath of matrix material subjected to axial tension. An elastoplastic, axisymmetric finite element analysis has been used. Curing residual stresses, and hygrothermal effects induced due to changes in service temperature and humidity, are included. The influence of the interface between the fibre and matrix material on the behaviour of propagating cracks is also studied. The concept of crack-growth resistance curves (K_R-curves) has been used to determine the point of crack instability. Results demonstrate the usefulness of the analytical model in understanding the role of the matrix material in the failure process of composites.

1. Introduction

Much of the further development and application of fibrous composites in aerospace structures now depends on their fracture characterization. Unfortunately, the fracture behaviour of these materials is not as straightforward as in the case of metals, which typically perform within the framework of linear elastic fracture mechanics (LEFM). A direct application of LEFM to composites is generally not appropriate because of the complex failure processes exhibited by these materials. However, LEFM concepts with some modification have been applied to composites by a number of investigators [1–7]. Two different approaches, i.e., macromechanical and micromechanical, have been adopted in deriving analytical models for fracture studies. The macromechanical models [1], which treat the composite as a homogeneous, anisotropic continuum, even when they agree reasonably well with experimental results, do not fully explain the physical failure mechanism associated with fracture. On the other hand, the micromechanical models [7–10] have the potential of accounting for the affects of material inhomogeneity, which is very important in understanding the basic failure processes.

A simple micromechanical model consisting of a single fibre in an annular sheath of matrix material, with a layer of interface material between the fibre and the matrix (Fig. 1), is presented here.

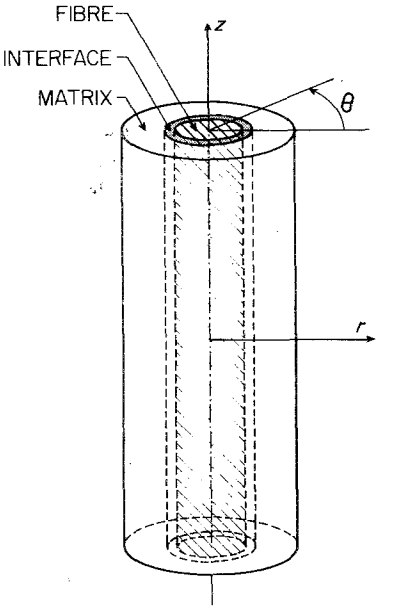

Figure 1 Axisymmetric micromechanical model.

0022–2461/83/020447–10$03.70/0

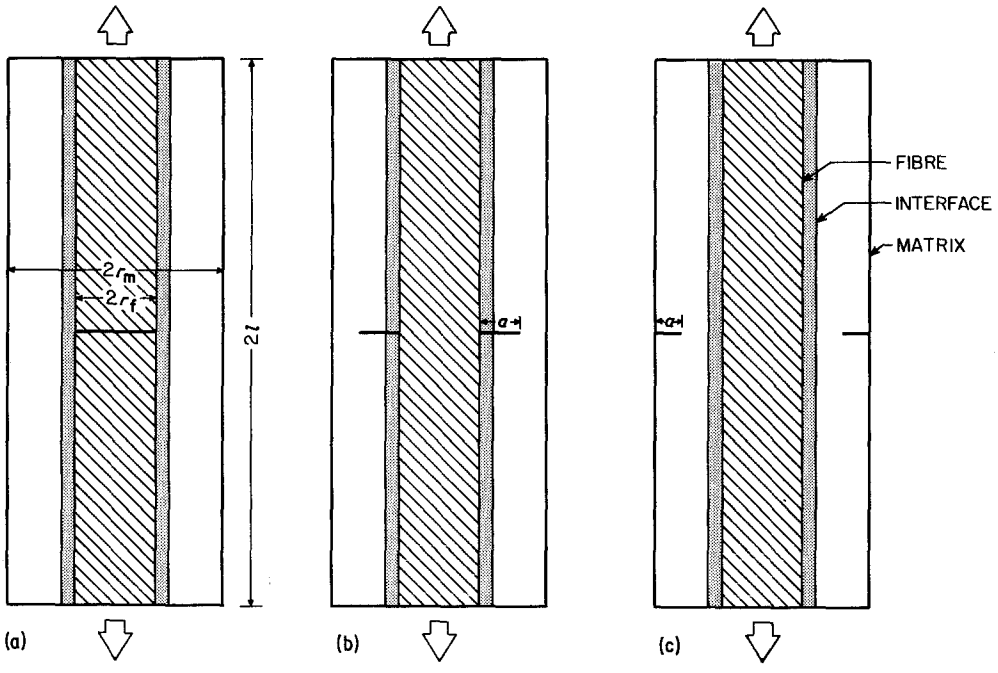

Figure 2 Cross-sections of three axisymmetric micromechanical fracture models. (a) Broken fibre, (b) matrix cracked adjacent to fibre, (c) matrix cracked away from fibre.

The analysis is focused on the problem of crack initiation and propagation in the epoxy matrix in a graphite/epoxy composite. Three basic types of inherent flaws (see Fig. 2), i.e. a broken fibre, a circumferential crack in the matrix adjacent to an intact fibre, and a cicumferential crack in the matrix away from an intact fibre, are considered as critical sources from which a crack may initiate and propagate across the matrix.

A literature review of micromechanical analyses of unidirectional composites as related to fracture studies is given by Murphy and Adams [8]. The axisymmetric, elastoplastic finite element method used in the present analysis is described in detail by the same authors [10]. The problem of crack initiation and propagation from a broken fibre end in a ductile metal matrix composite (boron/aluminium) has also been studied [6, 7], using a model similar to the one presented here.

The crack-growth resistance curve concept for homogeneous (metallic) ductile materials [11], which exhibit substantial amounts of stable, self-similar crack growth prior to catastrophic failure, has been extended to polymer–matrix composites by some authors [2–7], even though the failure in these materials is not governed by the same mechanisms. An energy absorption mechanism analogous to plastic flow in metals often takes place in composites, in the form of interfacial separation between the fibres and the matrix within individual plies, prior to fibre fracture and pull-out. The present micromechanical analysis is aimed at resolving this basic energy absorption mechanism in polymer–matrix composites.

2. Model geometry

The micromechanical model of a single fibre in an annular sheath of matrix material (Fig. 1), with any one of three different types of initial cracks (Fig. 2), has been modelled using the axisymmetric, triangular finite element grid shown in Fig. 3. Only one-half the length need be modelled, making use of the plane of symmetry at the initial crack plane. The l/r_m ratio of 4:1 used here has been shown [6] to be sufficient to avoid influences of end effects on stress distributions. The length of the initial crack was varied by changing the boundary conditions (and also the associated material type in the case of the broken fibre model), while maintaining the overall finite element grid. A total of 840 elements were used, with more than half of these elements concentrated near the crack plane. The failed element approach [8, 10] employed in the present analysis required a fine grid in the region of anticipated crack growth. The model also incorporates a double-node concept, at the junction

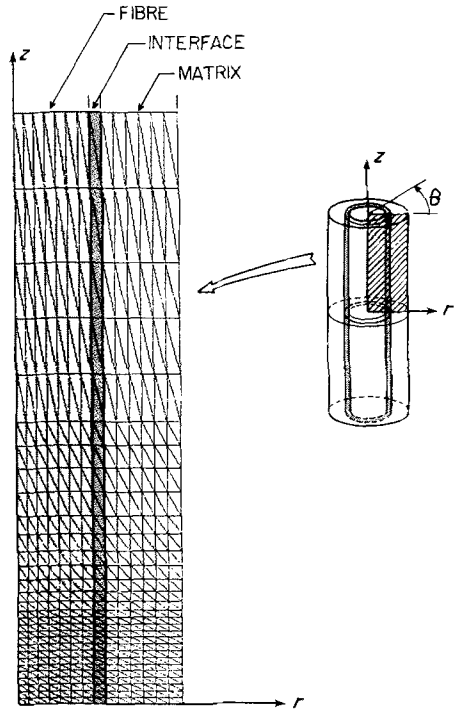

Figure 3 Finite element grid utilized.

of the broken fibre and the surrounding matrix, as described in detail by Adams and Mahishi [6]. This permits the representation of the actual conditions of total discontinuity of the fibre at the break, while retaining the continuity of the matrix material at the same point.

3. Material properties

The constituent materials used in the present investigation were Hercules 3501-6 epoxy matrix (a 177° C cure system) and Hercules AS graphite fibres (see Table I). The analysis takes into account the highly anisotropic nature of the graphite fibre (assuming it to be transversely isotropic). The matrix properties, presented previously [12, 13], were obtained using solid rod torsion tests. The data were obtained for dry specimens and specimens saturated with moisture, tested at three temperature conditions, i.e., 21° C (room temperature), 100° C and 160° C. The octahedral shear stress–octahedral shear strain relations derived from these tests are shown in Fig. 4. The non-linear temperature- and moisture-dependent

TABLE I Constituent material properties for Hercules AS graphite fibre and 3501-6 epoxy resin [12, 13]

Property	Hercules AS graphite fibre		Hercules 3501-6 epoxy matrix (room temperature, dry)	
Longitudinal modulus, E_l GPa (10^6 psi)	221	(32.0)	5.79	(0.84)
Tranverse modulus, E_t GPa (10^6 psi)	13.8	(2.0)	5.79	(0.84)
Longitudinal shear modulus, G_{lt} GPa (10^6 psi)	34.5	(5.0)	2.14	(0.31)
Transverse shear modulus, G_{tt} GPa (10^6 psi)	5.52	(0.80)	2.14	(0.31)
Major Poisson's ratio, ν_{lt}	0.20		0.34	
In-plane Poisson's ratio, ν_{tt}	0.25		0.34	
Longitudinal tensile strength, σ_l^u MPa (10^3 psi)	3103	(450.0)	170	(24.6)
Transverse tensile strength, σ_t^u MPa (10^3 psi)	345	(50.0)	170	(24.6)
Longitudinal shear strength, τ_{lt}^u MPa (10^3 psi)	1551	(225.0)	84.8	(12.3)
Transverse shear strength, τ_{tt}^u MPa (10^3 psi)	172	(25.0)	84.8	(12.3)
Longitudinal coefficient of thermal expansion, α_l (10^{-6} °C^{-1})	−0.36		40.0	
Transverse coeffient of thermal expansion, α_t (10^{-6} °C^{-1})	18.0		40.0	
Coefficient of moisture expansion, β (10^{-3} %M^{-1})	0		2.0	

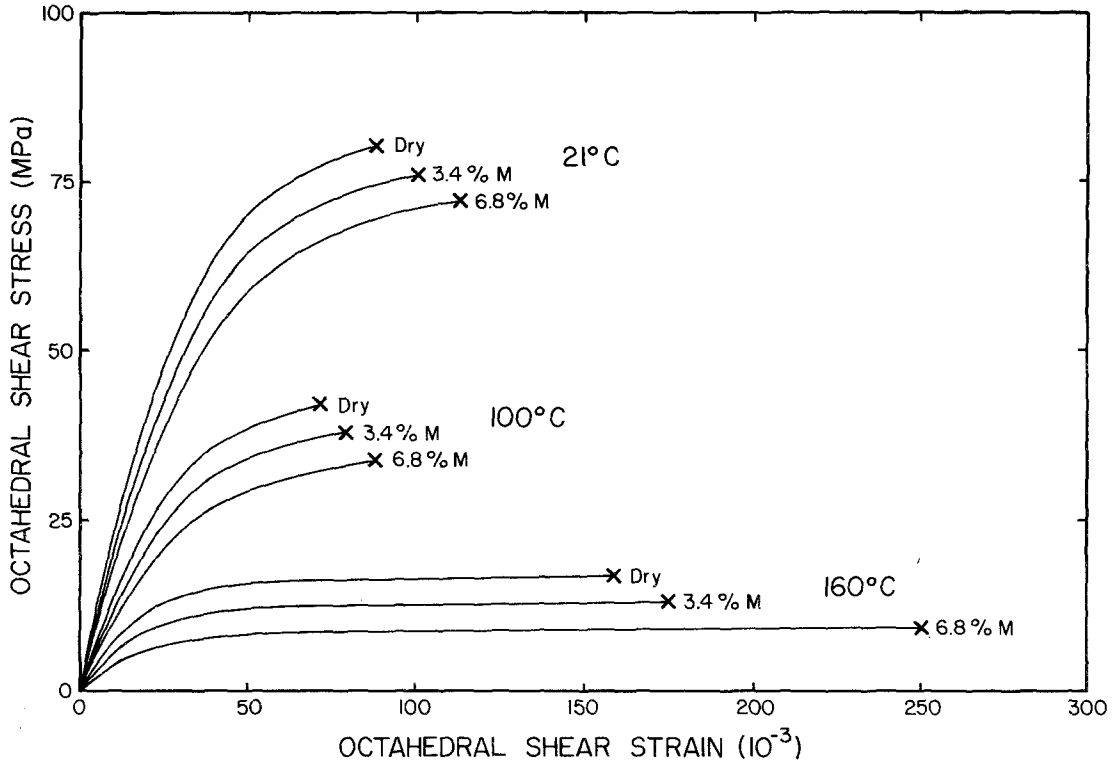

Figure 4 Hercules 3501-6 epoxy matrix octahedral shear stress–octahedral shear strain curves as generated from solid rod torsion tests [13]. (%M is the weight per cent moisture absorption.)

material properties are modelled in the present micromechanics analysis by expressing the stress–strain relations in equation form, using a curve-fitting method developed by Richard and Blacklock [14], which enables the computer program to calculate the tangent modulus at each load increment.

4. Crack initiation and propagation technique

The "failed element" crack initiation and propagation scheme used in the present analysis assumes that when an individual finite element exhausts all of its strain energy capacity it fails, forming a "crack". The failed element is then removed from the model by transferring the reaction loads of the failed element to adjacent elements and reducing its stiffness properties to zero. Depending on the stress state, the elements adjacent to a failed element may then fail when the reaction loads are applied. If the applied stress on the composite is held constant during this process of failure, elements may continue to fail, leading to catastrophic failure. In the present analysis, the crack growth is arrested, by restraining the loaded end of the model from displacement during the increment of crack growth. This results in a drop of the applied stress.

The crack initiation and propagation process strongly depends on the failure criterion used. Six different failure theories currently in common use are included in the present analysis. All six failure criteria were tested here, for the particular case of the broken fibre model with $r_f/r_m = 0.46$. The predicted crack initiation and ultimate stresses are compared in Table II. The maximum normal stress criterion was used in all other examples to be presented.

The crack-growth resistance curve method was used to determine the point of crack instability whenever a stable self-similar crack growth was observed. The K_R curves were obtained by evaluating the energy release rate G (normalized with respect to the radius defining the crack front), during each increment of crack growth, and using the relation $K_R = (E_c G)^{1/2}$, where E_c is the axial elastic modulus of the model composite.

5. Numerical results

Three different ratios of fibre radius, r_f, to matrix radius, r_m, i.e., $r_f/r_m = 0.25$, 0.46, and 0.84, were used to study the crack initiation and propagation

TABLE II Comparison of various failure criteria for axial tensile loading of a graphite/epoxy broken fibre model composite ($r_f/r_m = 0.46$)

Failure criterion	Predicted failure stresses (MPa)	
	Crack initiation	Ultimate strength
Maximum normal stress	39.3	98.2
Maximum shear stress	48.0	95.8
Octahedral shear stress	48.6	96.5
Hoffmann	9.1	44.6
Tsai–Hill	51.8	144.8
Tsai–Wu	10.2	40.2

in the case of the broken fibre model. Typical stress–strain responses are shown in Fig. 5. It should be noted that the stress and the strain plotted are the composite axial stress (the total applied force divided by the gross cross-sectional area of the model) and the composite axial stress (the ratio of the relative displacement of loaded boundary to the total length of the model).

In all the cases studied the composite was considered to be cured at a temperature of 177° C, then cooled to room temperature (21° C) before applying any temperature, moisture or axial load increments. The affect of the curing cycle, which induces negative axial (residual) strains in the composite, is shown in Fig. 5. It is also shown that this residual strain decreases as fibre content increases, as expected.

The first abrupt drop in the applied axial stress corresponds to crack initiation. It was observed in the case of the broken fibre model that the crack growth was slow initially (of the order of one element length in front of the crack for every one or two load increments). This was followed by a rapid growth of the crack, which propagated completely outward across the cross-section. The crack growth in the present study of a graphite/epoxy composite was much more rapid than that observed in the boron/aluminium composite [6, 7]. In the case of boron/aluminium, the crack growth across the aluminium matrix occurred in a greater number of smaller increments.

Fig. 6 shows the effect of temperature and moisture environmental conditions. Most of the curing residual strain is relieved when the composite is heated to the 160° C, dry condition; the 100° C, 6.8 wt% matrix moisture condition

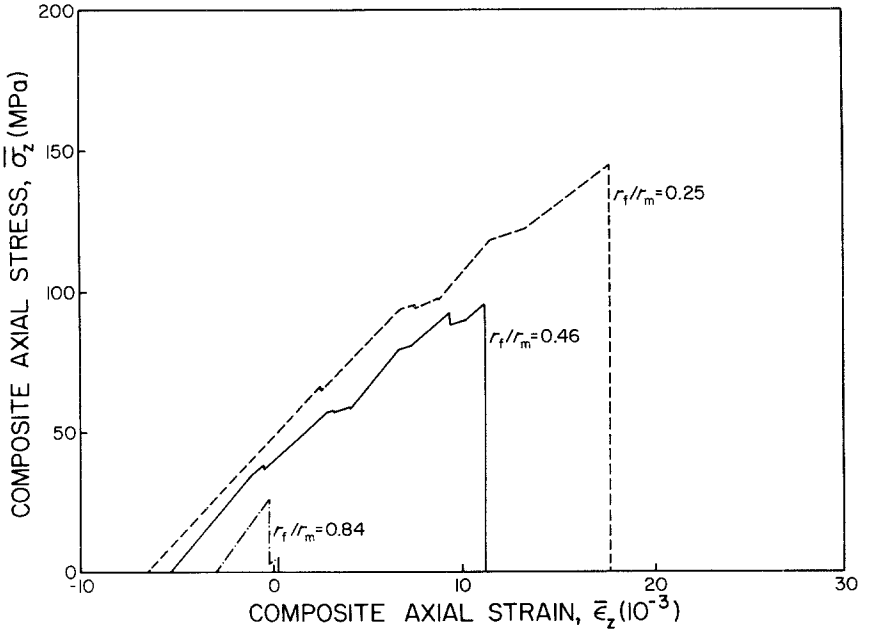

Figure 5 Stress–strain response of the broken fibre model at the room temperature, dry condition for three fibre/matrix radius ratios.

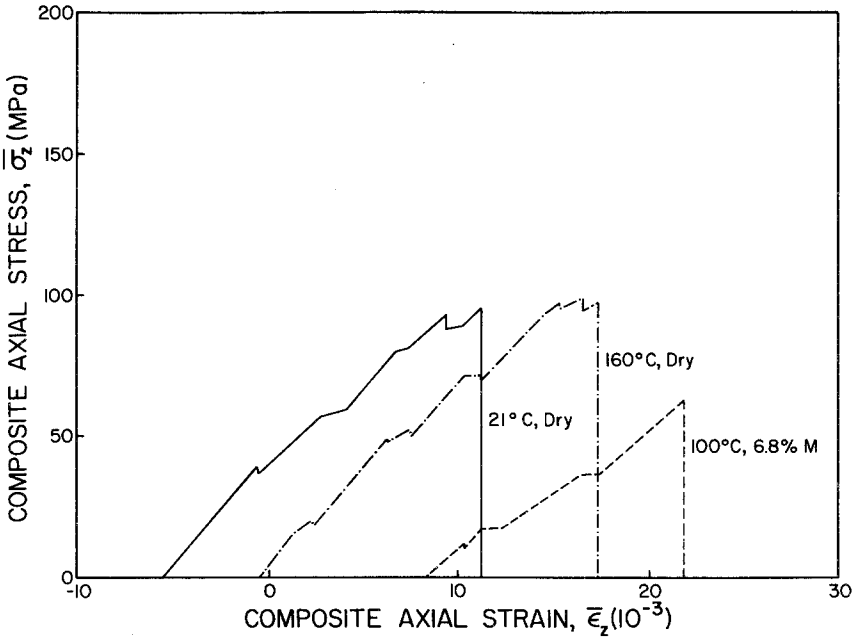

Figure 6 Stress–strain response of the broken fibre model at two non-ambient conditions, compared with the ambient condition, for $r_f/r_m = 0.46$.

induces a very large positive axial residual strain, due to the moisture-induced swelling of the epoxy matrix.

The predicted ultimate strengths for the various r_f/r_m ratios are plotted in Fig. 7. The extreme values, i.e., $r_f/r_m = 0$ and $r_f/r_m = 1$, correspond to the special cases of all matrix (without a crack) and a completely broken fibre and no matrix, respectively. The results of Fig. 7 suggest a linear relationship between the r_f/r_m ratio and ultimate strength.

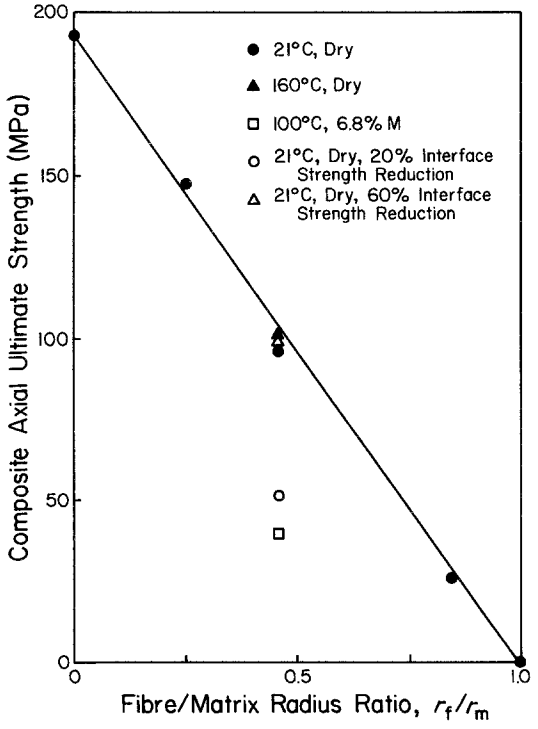

Figure 7 Plot of predicted ultimate strength against fibre/matrix radius ratio for the broken fibre model.

Fig. 7 also shows the affect of a weak interface between the fibre and matrix on the ultimate strength of the composite. It was observed in the case of the interface having only 80% of the matrix strength (i.e. a 20% reduction) that the crack initiated very early during the loading process, in an interface element at the broken fibre end, and propagated across the matrix without propagating along the interface. The predicted ultimate strength was significantly low (51.7 MPa). The response was quite different when the strength of the interface material was further reduced, to 40% of the matrix material strength (i.e. a 60% reduction). The affect was similar to the crack blunting which occurs in ductile metals due to plastic flow. The crack grew along the interface a substantial amount before propagating across the matrix. This is illustrated in Fig. 8.

The crack initiation and propagation in the matrix from the pre-existing circumferential cracks are shown in Figs. 9 and 10. Two different initial crack lengths were modelled in both the

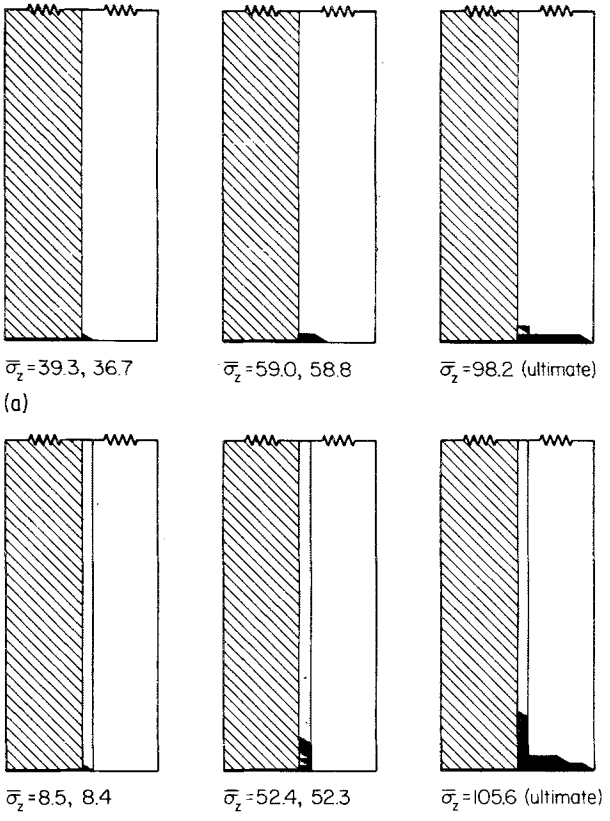

Figure 8 Crack propagation in a broken fibre model composite for the case of $r_f/r_m = 0.46$ (applied axial stresses, in MPa, before and after a crack growth increment are shown). (a) without interface layer, (b) with 60% reduced strength interface layer.

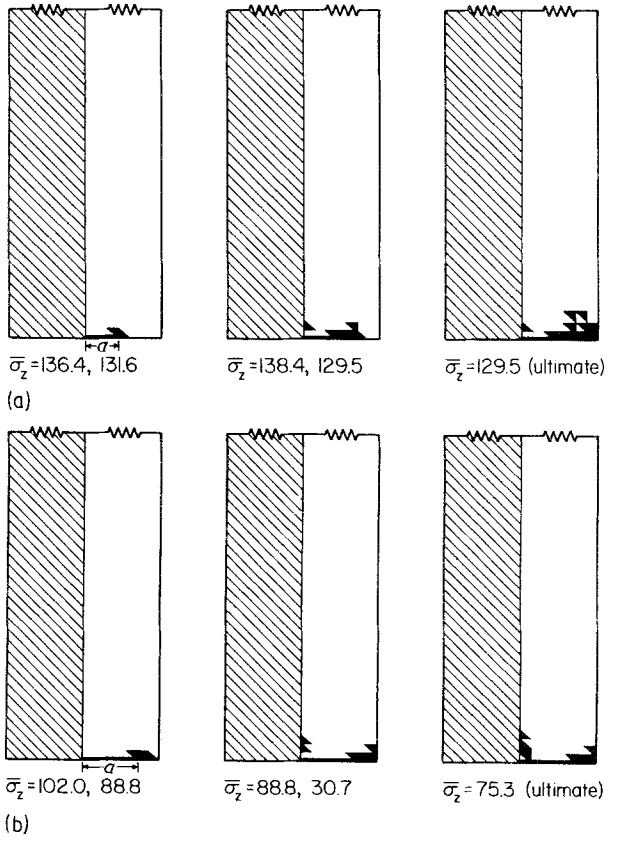

Figure 9 Crack propagation in an internally cracked matrix model for the case of $r_f/r_m = 0.46$ (applied axial stresses, in MPa, before and after a crack growth increment are shown). (a) $a/(r_m - r_f) = 0.27$; (b) $a/(r_m - r_f) = 0.70$.

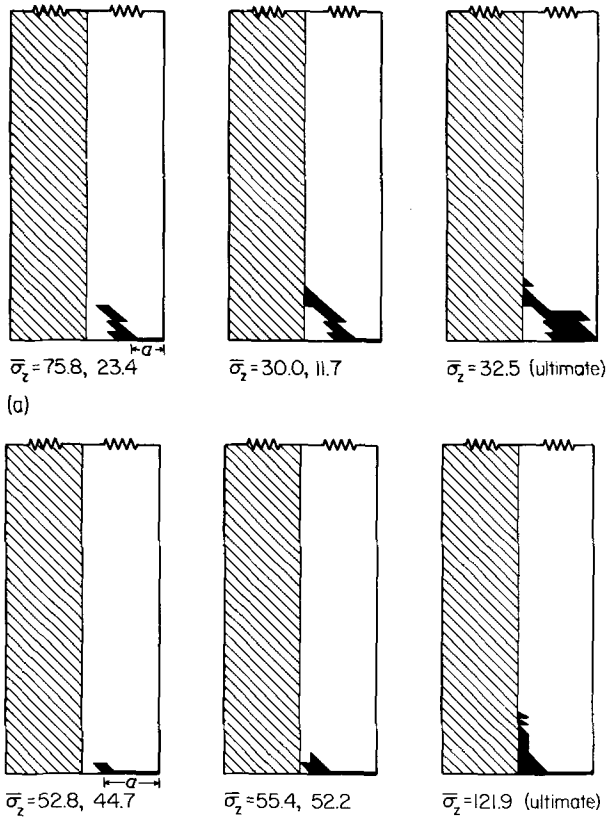

Figure 10 Crack propagation in an externally cracked matrix model for the case of $r_f/r_m = 0.46$ (applied axial stresses, in MPa, before and after a crack growth increment are shown). (a) $a/(r_m - r_f) = 0.30$; (b) $a/(r_m - r_f) = 0.73$.

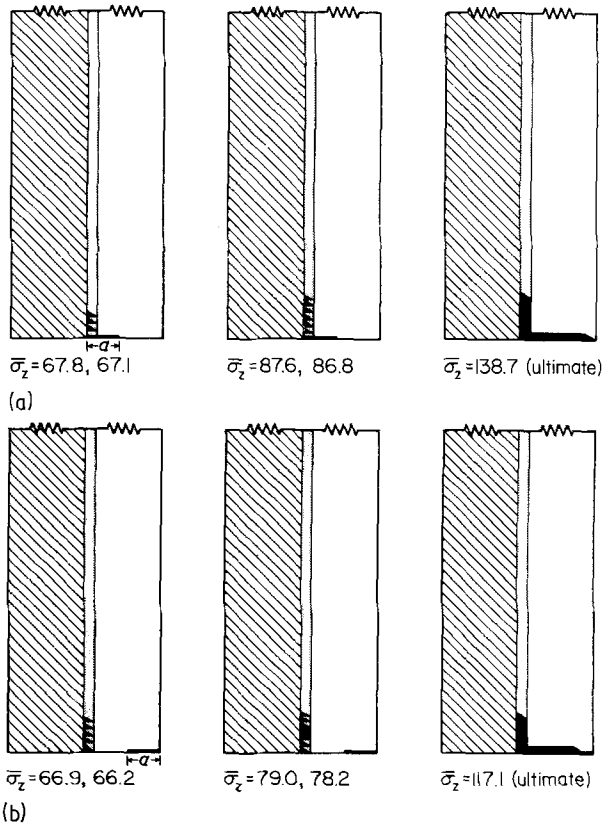

Figure 11 Crack propagation in cracked matrix, weak interface layer (60% reduced strength) models for the case of $r_f/r_m = 0.46$ (applied axial stresses, in MPa, before and after a crack growth increment are shown). (a) Internally cracked matrix, $a/(r_m - r_f) = 0.27$; (b) externally cracked matrix, $a/(r_m - r_f) = 0.30$.

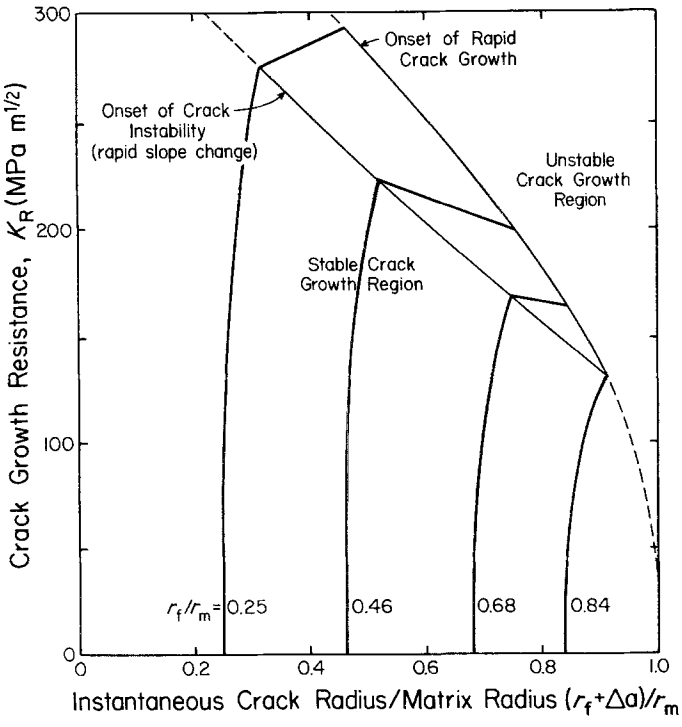

Figure 12 Crack growth resistance (K_R) curves for the broken fibre, no weak interface model.

cases, i.e. for a crack adjacent to the fibre and a crack away from the fibre. In general, the crack initiated at much higher applied stress levels compared to the case of a broken fibre, and propagated rapidly across the matrix, even though the applied stress continuously decreases. It will be noted in Fig. 10 that the crack growth was not self-similar in the case of the externally cracked matrix. The crack grew at an angle to the starting crack until it met the fibre, and then grew along the fibre interface.

The affect of a weak interface layer in the case of the cracked-matrix model (Fig. 11) was similar to that for the broken fibre model. The crack grew along the fibre a short distance before beginning to propagate across the matrix.

It was possible to apply the crack-growth resistance (K_R) curve concept only in the case of the broken fibre, no weak interface model, since only it exhibited relatively slow, self-similar crack growth. The K_R curves for four different r_f/r_m ratios are shown in Fig. 12. The points of crack instability determined by these K_R curves (points at which the slopes of the K_R curves abruptly change) occur much earlier in the loading process than do the points of initiation of rapid crack growth (failure of a large number of elements). Both of these definitions of instability are identified in Fig. 12. There are no known experimental data available at present to verify the analytical results presented here. Experiments using a physical model consisting of a graphite fibre embedded in an annular sheath of epoxy matrix would be very simple to perform.

Other micromechanical failure modes that are of practical interest include the post-debond sliding between fibre and matrix, fibre fracture, and fibre pull-out. These failure modes are discussed in greater detail by Beaumont and Anstice [15], and could also be modelled using the present analytical technique.

6. Conclusions

The micromechanical model presented here has been shown to be very useful in understanding the basic failure processes that take place in the matrix material in a polymer–matrix composite. The requisite experiments for verification and correlation purposes are simple, and will be relatively easy to perform. The analysis could serve as a useful screening mechanism as new polymers are developed for uses in composites.

Acknowledgements

The present study was performed under the sponsorship of the Army Research Office, Dr John C. Hurt, Grant Monitor, using analysis techniques developed in part of a NASA-Lewis grant, Dr James A. DiCarlo, Grant Monitor.

References

1. M. E. WADDOUPS, J. R. EISENMANN and B. E. KAMINSKI, *J. Comp. Mater.* **5** (1971) 446.
2. S. GAGGAR and L. J. BROUTMAN, *ibid.* **9** (1975) 216.
3. D. H. MORRIS and H. T. HAHN, "Composite Materials: Testing and Design", ASTM STP 617 (ASTM, Philadelphia, 1977) p. 5.
4. A. C. GARG, *Fibre Sci. Tech.* **14** (1981) 27.
5. S. OCHIAI and P. W. M. PETERS, *J. Mater. Sci.* **17** (1982) 417.
6. D. F. ADAMS and J. M. MAHISHI, University of Wyoming, USA, Report UWME-DR-201-101-1 (1982).
7. J. M. MAHISHI and D. F. ADAMS, *J. Comp. Mater.* **16** (1982) in press.
8. D. P. MURPHY and D. F. ADAMS, University of Wyoming, USA, Report UWME-DR-901-103-1 (1979).
9. J. G. GOREE and R. S. CROSS, *J. Eng. Frac. Mech.* **13** (1980) 563.
10. D. F. ADAMS and D. P. MURPHY, University of Wyoming, USA, Report UWME-DR-101-102-1 (1981).
11. R. H. HEYER, ASTM STP 527 (ASTM, Philadelphia, 1973) p. 3.
12. G. C. GRIMES, D. F. ADAMS and E. G. DUSABLON, Northrop Corp./University of Wyoming, USA, Report NOR-80-158 (1980).
13. D. A. CRANE and D. F. ADAMS, University of Wyoming, USA, Report UWME-DR-101-101-1 (1981).
14. R. M. RICHARD and J. R. BLACKLOCK, *AIAA J.* 7 (1969) 432.
15. P. W. R. BEAUMONT and P. D. ANSTICE, *J. Mater. Sci.* **15** (1980) 2619.

Received 22 June
and accepted 12 July 1982